Kinetic Turbulence in Astrophysical Plasmas: Waves and/or Structures?

Daniel Grošelj,[1] Christopher H. K. Chen,[2] Alfred Mallet,[3] Ravi Samtaney,[4] Kai Schneider,[5] and Frank Jenko[1]

[1]*Max-Planck-Institut für Plasmaphysik, D-85748 Garching, Germany*
[2]*School of Physics and Astronomy, Queen Mary University of London, London E1 4NS, UK*
[3]*Space Science Center, University of New Hampshire, Durham, NH 03824, USA*
[4]*Mechanical Engineering, King Abdullah University of Science and Technology, Thuwal 23955-6900, Saudi Arabia*
[5]*I2M-CNRS, Centre de Mathématiques et d'Informatique, Aix-Marseille Université, 13453 Marseille Cedex 13, France*

(Dated: June 18, 2018)

The question of the relative importance of coherent structures and waves has for a long time attracted a great deal of interest in astrophysical plasma turbulence research, with a more recent focus on kinetic scale dynamics. Here we utilize high-resolution observational and simulation data to investigate the nature of waves and structures emerging in a weakly collisional, turbulent kinetic plasma. Observational results are based on *in situ* solar wind measurements from the Cluster and MMS spacecraft, and the simulation results are obtained from an externally driven, three-dimensional fully kinetic simulation. Using a set of novel diagnostic measures we show that both the large-amplitude structures and the lower-amplitude background fluctuations preserve linear features of kinetic Alfvén waves to order unity. This quantitative evidence suggests that the kinetic turbulence cannot be described as a mixture of mutually exclusive waves and structures but may instead be pictured as an ensemble of localized, anisotropic wave packets or "eddies" of varying amplitudes, which preserve certain linear wave properties during their nonlinear evolution.

I. INTRODUCTION

The nature of weakly collisional, kinetic scale plasma turbulence is presently one of the outstanding problems in space and astrophysical plasmas, with important implications for the turbulent heating of ions and electrons [1–4]. In resemblance with a wider class of turbulent systems, such as rotating fluid flows [5, 6] or turbulent surface waves [7], plasma turbulence is often pictured either as a superposition of interacting waves or, alternatively, as a collection of localized coherent structures [8]. A series of compelling questions emerge in this context such as: Which of these two aspects, structures or waves, is more essential and/or fundamental to the turbulent dynamics? And also: Are waves and structures mostly exclusive to each other and simply "coexist" in the turbulence or is there a deeper connection between the two? In this paper we straightforwardly address these open questions in the context of kinetic plasma turbulence, where the topic of waves and structures is hotly debated at present [9–18]. To this end, we introduce a set of novel diagnostic measures, appropriate for the study of waves and structures in a kinetic plasma, such as the weakly collisional solar wind [19]. The general approach outlined in this paper and the conclusions drawn from it are, however, not exclusively limited to kinetic scale plasma turbulence and could be applicable to a wide range of turbulent regimes and environments where waves and structures can be identified [5–7, 20].

Different theoretical concepts have been considered to explain the properties of weakly collisional plasma turbulence at kinetic scales below the ion thermal gyroradius. A common approach relies on the use of linearized kinetic equations [10, 21–24]. The use of linear theory is motivated empirically by the relatively successful history of the method in observational studies and simulations, often showing reasonable agreement with linear predictions even in strongly turbulent regimes [13, 17, 25–29]. Theoretically, the motivation is based on the premise of critical balance [21, 22, 30, 31]. This assumes—to order unity—a balance between the characteristic nonlinear (eddy turnover) and linear (wave crossing) time in regimes of strong plasma turbulence. Complementary to linear treatments, several authors have emphasized the role of intermittency and the nonlinear generation of turbulent structures (e.g., [16, 32–34]), such as current sheets [14, 35–37], Alfvén vortices [16, 38], or magnetic holes [39, 40]. Indeed, *in situ* solar wind measurements [16, 36, 38, 41] and numerical simulations [12, 15, 18, 32, 33, 35, 42] support the idea that kinetic scale coherent structures emerge naturally as a result of the turbulent cascade. Yet, it is presently not well understood how these localized structures impact the global dynamics and turbulent dissipation, or the wavelike properties of the kinetic cascade. Moreover, no general consensus presently exists within the field regarding the question on the relative importance of waves and structures.

Despite being of quite general theoretical interest, the topic of kinetic plasma turbulence has seen a burst of activity only recently due to the advances in state-of-the-art observational and computational techniques. This includes, among others, high-resolution, *in situ* solar wind measurements [13, 36, 43–46], supplemented by massively parallel, first principles kinetic simulations in three spatial dimensions [15, 17, 47, 48]. It is anticipated that detailed studies of turbulence in the observationally accessible solar wind can provide valuable insight into a wide range of turbulent astrophysical plasmas [19], such as galaxy clusters [3, 49], accretion disks [1, 50], and the warm interstellar medium [51]. Here, we combine the state-of-the-art observational and computational approaches to examine the relationship between waves and turbulent structures at kinetic scales below the ion thermal gyroradius. Observational results are based on solar wind measurements from the Cluster and MMS spacecraft, whereas the numerical results are obtained from an externally driven, three-dimensional (3D) fully kinetic particle simulation. We jointly analyze the observational and simulation data using a set of new diagnostic measures. In par-

ticular, we introduce appropriate generalizations of so-called spectral field ratios in order to study the interplay between high-amplitude, intermittent fluctuations and wavelike properties.

In the following, we employ the generalized field ratios to show that the large-amplitude localized fluctuations preserve linear features of kinetic Alfven waves (KAWs) [10, 21–23] to order unity. This result is obtained despite the fact that the scale-dependent magnetic field and electron density fluctuations each separately display signatures of non-Gaussian statistics, typically attributed to the presence of coherent structures. Furthermore, an analysis of simulation data suggests that the intermittency emerges mainly due to a mixture of sheetlike and filamentary, pressure-balanced structures extending down to electron scales. Based on quantitative evidence, we conclude that the turbulent structures themselves may carry linear wave signatures.

The paper is organized as follows. In Sec. II we briefly summarize the linear KAW theoretical predictions. The methods employed are described in Sec. III. This includes a brief overview of a new high-resolution 3D fully kinetic simulation, a description of observational data, a summary of wavelet scale decompositions, and finally, the generalized field ratio definitions. Our main results are presented in Sec. IV. We conclude the paper with a discussion and summary of our results in Sec. V.

II. THEORY

We use the KAW turbulence theory [21–23] as the main basis for making contact with linear predictions. This is motivated by recent works on solar wind turbulence (e.g., [13, 17, 25]), showing reasonable agreement with linear predictions for KAWs. The choice can be further justified *a posteriori* based on our results which render known alternatives, such as whistler wave turbulence [10, 52–54], less suitable. The fluidlike equations underlying the theory of KAW turbulence admit a natural normalization [13, 23, 55] for the magnetic field ($\delta\mathbf{b}$) and electron density (δn_e) fluctuations given by

$$\delta n_e' = \left[\frac{\beta_i+\beta_e}{2}\left(1+\frac{\beta_i+\beta_e}{2}\right)\right]^{1/2}\frac{\delta n_e}{n_0}, \tag{1}$$

$$\delta\mathbf{b}_\perp' = \frac{\delta\mathbf{b}_\perp}{B_0}, \tag{2}$$

$$\delta\mathbf{b}_\parallel' = \left(\frac{2+\beta_i+\beta_e}{\beta_i+\beta_e}\right)^{1/2}\frac{\delta\mathbf{b}_\parallel}{B_0}, \tag{3}$$

where n_0 is the mean density, B_0 is the mean magnetic field strength, $\beta_i = 8\pi n_0 T_i/B_0^2$ and $\beta_e = 8\pi n_0 T_e/B_0^2$ are the ion and electron betas, and T_i and T_e are the ion and electron temperatures (measured in energy units), respectively. The subscripts $\perp$ and $\parallel$ denote components perpendicular and parallel to the mean magnetic field. The normalizations are such that the KAW fluctuation amplitudes obey the following relations:

$$\left|\delta n_e'\right|^2 = \left|\delta\mathbf{b}_\perp'\right|^2 = \left|\delta\mathbf{b}_\parallel'\right|^2 = \mathcal{E}'_{\rm KA}/2, \tag{4}$$

where $\mathcal{E}'_{\rm KA} = \left|\delta\mathbf{b}_\perp'\right|^2 + \left|\delta n_e'\right|^2$ is the KAW energy density [23]. The above equalities form the basis for our identification of kinetic-Alfvén wavelike properties [56]. The analytical expressions (4) are derived for a $\beta \sim 1$ plasma in the asymptotic limit

$$1/\rho_i \ll k_\perp \ll 1/\rho_e, \qquad k_\parallel \ll k_\perp, \tag{5}$$

where $k_\parallel$ is the parallel wave number, $k_\perp$ is the perpendicular wave number, ρ_i is the ion thermal gyroradius, and ρ_e is the electron thermal gyroradius [57]. We note that (4) is obtained for a given Fourier mode but does not guarantee an analogous relation in real space for systems populated by many KAWs with different wave numbers. There exists, however, a second linear relation which can be written in real space:

$$\delta n_e'(\mathbf{r}) = -\delta b_\parallel'(\mathbf{r}). \tag{6}$$

The above is a result of a balance between the perpendicular kinetic and magnetic pressures [22]. On the other hand, no general linear relation, similar to Eq. (6), exists between $\delta\mathbf{b}_\perp'$ and $\delta n_e'$ (or $\delta\mathbf{b}_\parallel'$) in real space, although a spatial coupling can be induced nonlinearly [32, 58]. Note that, in a *single* KAW, the field-perpendicular magnetic fluctuations are simply shifted in phase by 90 degrees relative to the density, owing to the elliptical polarization of the KAW [22]. We do not restrict ourselves here to the case of monochromatic waves with a well-defined (single) wave number and frequency. On the contrary, our main interest is the regime of strong turbulence, where a wavelike description can be given in terms of localized wave packets consisting of many different modes. From here on, we drop the prime signs but it is to be understood that all fields are normalized according to (1)-(3) unless noted otherwise.

III. METHODS

Below we describe the numerical simulation and observational data, the data analysis techniques, and introduce the generalized field ratios. These aspects are essential for a complete understanding of this work. However, those interested only in the main outcome of the study may skip over to the results in Sec. IV.

A. Driven 3D fully kinetic simulation

The simulation results are obtained from a high-resolution, 3D fully kinetic simulation. In contrast with the few existing 3D fully kinetic simulations of sub-ion range turbulence (e.g., [15, 17, 40]), we present here the first such simulation with an external forcing. We perform the simulation using the particle-in-cell code OSIRIS [59, 60]. The periodic domain size is $(L_x, L_y, L_z) = (18.9,\ 18.9,\ 48.3)\, d_i$, where $d_i = \rho_i/\sqrt{\beta_i}$ is the ion inertial length. The global mean field $\mathbf{B}_0$ points in the z direction. The spatial resolution is $(N_x, N_y, N_z) = (928, 928, 1920)$ with 150 quadratic-spline-shaped particles per cell per species. A reduced ion-electron mass ratio of $m_i/m_e = 100$ is used and the electron plasma to cyclotron

frequency ratio is $\omega_{pe}/\Omega_{ce} = 2.86$. To reduce particle noise, the output fields used for the analysis are short-time averaged over a window of duration $\Delta t\Omega_{ce} = 2.0$, where Ω_{ce} is the electron cyclotron frequency. Following Ref. [48], the forcing is an adaptation of the Langevin antenna [61] and introduces a time-dependent external electric current $\mathbf{J}_{\rm ext}$. We apply $\mathbf{J}_{\rm ext}$ at wave numbers $(1, 0, \pm 1)$, $(0, 1, \pm 1)$, $(-1, 0, \pm 1)$, and $(0, -1, \pm 1)$ in units of $(2\pi/L_x,\, 2\pi/L_y,\, 2\pi/L_z)$. The antenna current is divergence free and drives low-frequency Alfvénic fluctuations. To avoid a rapid transient response, we initialize the fluctuating field at $t = 0$ to match the external current via $\nabla \times \delta\mathbf{b}_\perp = (4\pi/c)\mathbf{J}_{\rm ext}$. We choose an antenna frequency $\omega_0 = 0.9 \cdot (2\pi v_A/L_z)$, where $v_A = B_0/\sqrt{4\pi n_0 m_i}$ is the Alfvén speed, and the decorrelation rate [61] is $\gamma_0 = 0.6\omega_0$. The ion and electron velocity distributions at $t = 0$ are isotropic Maxwellians with $\beta_i \approx \beta_e \approx 0.5$.

The approach towards a statistically steady state is depicted in Fig. 1. The simulation is run for about 2.24 Alfvén transit times, $t_A = L_z/v_A$, until the kinetic scale spectra appear to be converged. At the end of the simulation, the mean ion and electron betas (based on their space-averaged local values) are $\beta_i = 0.56$ and $\beta_e = 0.51$. The turbulence is strongly driven such that $\delta b^{\rm rms} \approx L_\perp/L_z \approx 0.4$ towards the end of the simulation [Fig. 1(a)], where $\delta b^{\rm rms}$ is the root-mean-square fluctuating field in units of B_0. This corresponds to critical balance ($\delta b^{\rm rms} \approx k_\parallel/k_\perp$) at the forced wave numbers. The one-dimensional (1D) magnetic energy spectrum as a function of $k_\perp \equiv (k_x^2 + k_y^2)^{1/2}$ [Fig. 1(b)] exhibits an approximate power law with a steepening of the spectral exponent close to electron scales. The spectrum is consistent with solar wind measurements, which typically show spectral exponents around -2.8 at sub-ion scales, while steeper exponents are measured close to electron scales and beyond [43, 45]. In the inset of Fig. 1(b) we show for reference the 1D k_z spectrum. To further reduce contributions from particle noise in the subsequent analysis, we filter out the noise dominated modes with $k_z d_i > 12$ [62].

Employing the method of Cho and Lazarian [55], we consider in Fig. 2 the anisotropy relative to the *local* mean field. The sub-ion range anisotropy, $k_\parallel(k_\perp)$, is scale-dependent and has a slope of approximately 1/3 on the logarithmic graph, in agreement with a recent fully kinetic simulation of decaying turbulence [17]. According to the asymptotic KAW theory for a $\beta \sim 1$ plasma [23], KAWs are expected to exist for wave numbers with $k_\parallel/k_\perp \ll 1$ and $k_\parallel d_i \ll 1$. While these values are not asymptotically small in our simulation, the anisotropy curve is well within the range $k_\parallel/k_\perp < 1$ and $k_\parallel d_i < 1$ at sub-ion scales. We also estimate the ratio of linear (KAW) to nonlinear time scales [Fig. 2(b)], given by $\chi = \tau_{\rm L}/\tau_{\rm NL} \approx \delta b_{\perp,k_\perp} k_\perp/(B_0 k_\parallel)$ [21, 22], where $\delta b_{\perp,k_\perp}$ is a scale-dependent fluctuation amplitude obtained from a sharp band-pass filter between $k_\perp/2$ and $2k_\perp$ [17]. The ratio of linear to nonlinear time scales is very close to unity around $k_\perp \rho_i \approx 1$ and exhibits a slight decline throughout the sub-ion range. As implied by this simple estimate, it appears that the kinetic scale nonlinear effects are not any more significant than linear physics even though the fluctuations are not small compared to the background [Fig. 1(a)]. These circumstances provide additional motivation for comparison with linear KAW predictions.

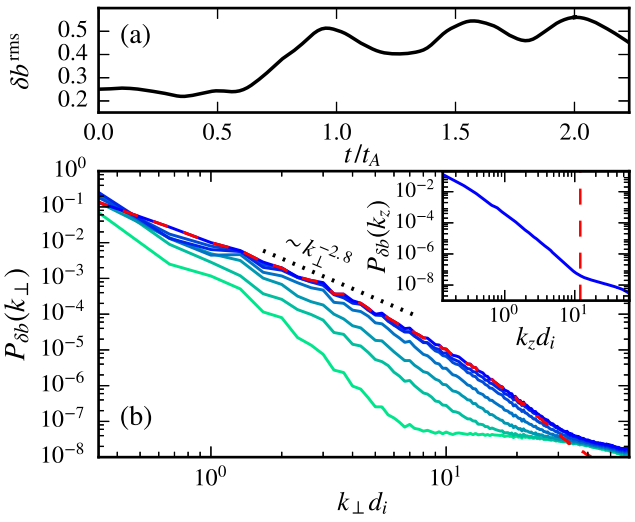

Figure 1. Time trace of the root-mean-square fluctuating magnetic field (a) and the 1D $k_\perp$ magnetic spectra at times $t/t_A = \{0.66, 0.92, 1.18, 1.45, 1.71, 1.97, 2.24\}$ in the simulation (light green to dark blue). A -2.8 slope is shown for reference (dotted line). The inset shows the k_z spectrum. Particle noise dominated modes with $k_z d_i > 12$ (vertical dashed line) are filtered out in the subsequent analysis. The k_z filtered $k_\perp$ spectrum at $t/t_A = 2.24$ is shown with a red dashed line in panel (b). All components of $\delta\mathbf{b}$ are normalized here to B_0.

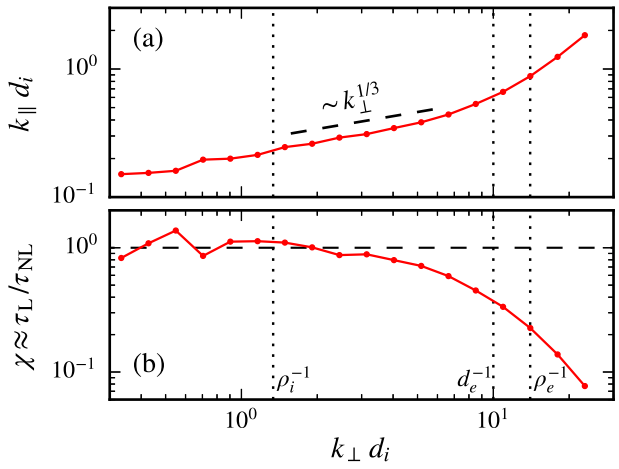

Figure 2. Local anisotropy of the externally driven turbulence (a) and the ratio of linear to nonlinear time scales (b). The 1/3 slope in panel (a) is shown for reference. All components of $\delta\mathbf{b}$ were normalized to B_0 in the anisotropy calculation.

B. Spacecraft data

The solar wind data analysis is based on a 7 h interval from the Cluster spacecraft [63] and on a 159 s interval from the Magnetospheric Multiscale (MMS) mission [64]. These inter-

vals were previously studied by Chen *et. al* [65] and Gershman *et. al* [46], respectively. At the time of the measurement, the Cluster spacecraft were in the free solar wind far from the Earth's foreshock, whereas the MMS spacacraft were in the Earth's magnetosheath but well separated from the bow shock and the magnetopause. The mean plasma betas are $\beta_i \approx 0.26$ and $\beta_e \approx 0.62$ for Cluster and $\beta_i \approx 0.27$ and $\beta_e \approx 0.03$ for the MMS interval. The analyzed data includes magnetic measurements from Cluster [65] and the electron density and magnetic measurements from MMS [46]. We convert the spacecraft frame frequencies $f_{\rm sc}$ to field-perpendicular wave numbers using Taylor's hypothesis [66]: $k_\perp \approx 2\pi f_{\rm sc}/v_0$, where v_0 is a characteristic velocity. We take v_0 to be the magnitude of the mean solar wind speed $\mathbf{V}_{\rm SW}$ for the Cluster interval. Given the relatively small angle between $\mathbf{B}_0$ and $\mathbf{V}_{\rm SW}$ during the MMS interval, we take $v_0 \approx |\mathbf{V}_{\rm SW}|\cos(\theta)$ for the MMS data, where $\theta \approx 76^\circ$ is the mean angle between $\mathbf{V}_{\rm SW}$ and the wave vector $\mathbf{k}$, determined in Ref. [46] using the k-filtering technique. This angle was found to be relatively constant throughout the entire kinetic range. The inferred mean angle between $\mathbf{k}$ and $\mathbf{B}_0$, on the other hand, was very close to 90 degrees [46]. To avoid edge effects, we skip a certain amount of points at the edges of the analyzed intervals when computing the wavelet based diagnostics (see Sec. III C). In particular, we skip about 5 s on each side of the Cluster interval and about 7 s on each side of the MMS interval.

The MMS interval covers around 80 ion inertial lengths in the field-perpendicular direction. This is too short to allow for a statistically reliable analysis of intermittency and the results are included here only for reference. Nevertheless, we still use the MMS data in order to be able to analyze simultaneous magnetic field and density measurements, which is crucial for making direct contact with the KAW predictions, where density fluctuations play a major role [13, 23]. Much longer suitable intervals from MMS are presently not available [46]. While the MMS interval is shorter than the typical large scale turbulence correlation time (e.g., [14]), the Cluster interval features a relatively long continuous stream of measurements, covering several correlation times. It is thus appropriate for studying intermittency, albeit with the limitation that only the magnetic measurements are available in this case.

C. Local scale extraction and generalized field ratios

The fields are decomposed locally among scales using 1D and two-dimensional (2D) complex-valued, continuous Morlet wavelet transforms [67–69]. The 1D transform is used for solar wind time trace measurements, and the 2D transform is used to analyze the simulation data at different x–y planes perpendicular $\mathbf{B}_0 = B_0\hat{\mathbf{e}}_z$. The 1D and 2D wavelet basis functions, ψ^{1D} and ψ^{2D}, can be represented explicitly in spectral space as band-pass filters of the following form

$$\widehat{\psi}_s^{1D}(k) = \Theta(k)\exp\left(\frac{-(k-k_s)^2}{2(k_s/k_0)^2}\right), \tag{7}$$

$$\widehat{\psi}_{s,\phi}^{2D}(k_x,k_y) = \exp\left(\frac{-(k_x-k_s\cos\phi)^2}{2(k_s/k_0)^2}\right) \times \exp\left(\frac{-(k_y-k_s\sin\phi)^2}{2(k_s/k_0)^2}\right), \tag{8}$$

where $\Theta(k) = 1$ for $k > 0$ and 0 otherwise, $k_0 = 6$ is a parameter [67], k_s is a characteristic wave number scale, and ϕ determines the angle in the x–y plane. Additionally, we impose $\widehat{\psi}_{s,\phi}^{2D}(0,0) = 0$. The variable k_s is related to the wavelet scale s via $k_s = k_0/s$. For some field $f(\mathbf{r})$, the Morlet wavelet coefficients $\widetilde{f}_s(\mathbf{r})$ at scale s are obtained from the inverse Fourier transform of $\widehat{f}\,\widehat{\psi}_s$, where $\widehat{f}$ is the Fourier transform of f. The set of wave number scales $\{k_s\}$ is logarithmically spaced and we use 12 angular directions $\phi \in [0,\pi)$ for the 2D transform. The results are later averaged over different angles. We define a local, scale-dependent fluctuation as $\delta f_s(\mathbf{r}) = c_1\Re\{\widetilde{f}_s\}$, where $\Re\{\dots\}$ is the real part. Similarly, we define a local power spectral density as $P_f(k_s,\mathbf{r}) = c_2\left|\widetilde{f}_s\right|^2/k_s$. The angular averaging of the local spectrum is performed after taking the squared modulus of the wavelet coefficient [69]. The normalization constants c_1 and c_2 may be determined based on the exact parameters of the wavelet transform [67, 68]. We leave these undetermined since our results do not dependent on such constant prefactors in the definitions of δf_s and P_f. In the following, we drop the scale subscript s but it is to be understood that all quantities are scale dependent.

We use the wavelet decomposition to define a new set of statistical measures. In particular, we consider the spectral field ratios, frequently used to study wave properties [10, 13, 25, 29, 70], and generalize their definitions to investigate the impact of high-amplitude, turbulent structures on these ratios. Two sets of generalized ratios are defined. The first set is based on the scale-dependent moments [71] of the fluctuations:

$$\left(\frac{\langle|\delta n_e|^m\rangle}{\langle|\delta b_\perp|^m\rangle}\right)^{2/m}, \quad \left(\frac{\langle|\delta n_e|^m\rangle}{\langle|\delta b_\parallel|^m\rangle}\right)^{2/m}, \quad \left(\frac{\langle|\delta b_\parallel|^m\rangle}{\langle|\delta b_\perp|^m\rangle}\right)^{2/m}, \tag{9}$$

where m is the order of the moment and $\langle\dots\rangle$ represents a space average. An additional angular average is performed after taking the space average when using 2D wavelets. The parallel and perpendicular fluctuations are defined here everywhere relative to the *local* mean field $\mathbf{B}_{\rm loc}$ as $\delta b_\parallel = \delta\mathbf{b}\cdot\mathbf{B}_{\rm loc}/|\mathbf{B}_{\rm loc}|$ and $\delta b_\perp = (\delta b^2 - \delta b_\parallel^2)^{1/2}$ [26, 72]. The local mean field is obtained from a Gaussian low-pass filter with a standard deviation $\sigma_s = k_s/k_0$ in spectral space. Once the parallel and perpendicular components have been determined, we normalize the fluctuations according to (1)-(3). For $m = 2$ the moment ratios yield the standard spectral ratios, defined in terms of the 1D $k_\perp$ spectra. On the other hand, for $m > 2$ the averaging becomes progressively more sensitive to the fluctuations at the tails of the probability distribution function, thus giving insight into

the dependence of the ratios on high-amplitude events. We consider moments up to $m = 6$.

Caution is needed when computing high-order statistics from finite data sets, since the tails of the probability distribution function may not be sufficiently sampled [73, 74]. For example, an estimate of the maximal moment $m_{\max}$ that can be determined accurately, based on the method presented in Ref. [73], yields typical values of $m_{\max}$ between 3 and 4 for the Cluster interval (with $N \approx 6.3 \times 10^5$ samples). To obtain more reliable estimates, we employ the scheme of Kiyani *et al.* [74] (see also Ref. [75]) and remove a small fraction of the largest fluctuations at each scale until the moments appear reasonably converged. For Cluster we find that removing 0.005% (i.e., about 30 samples) of largest fluctuations seems to be adequate. For consistency, we clip the same small fraction in the simulation when calculating the moments. Within the statistical uncertainties, the clipping does not significantly affect the results and only makes it easier to recognize true statistical trends. Due to the short duration of the MMS interval, the 0.005% clipping threshold has no effect and relatively large fractions would have to be removed to make the moments well behaved. Thus, no attempt is made to recover more reliable estimates via clipping for the MMS interval.

The ratios introduced in (9) are global measures in a sense that the average is taken over the entire volume. A more local measure can be obtained via conditional averaging of the local power spectral densities:

$$\frac{\langle|\widetilde{n}_e|^2\,|\mathrm{LIM}>\xi\rangle}{\langle|\widetilde{b}_\perp|^2\,|\mathrm{LIM}>\xi\rangle},\quad \frac{\langle|\widetilde{n}_e|^2\,|\mathrm{LIM}>\xi\rangle}{\langle|\widetilde{b}_\parallel|^2\,|\mathrm{LIM}>\xi\rangle},\quad \frac{\langle|\widetilde{b}_\parallel|^2\,|\mathrm{LIM}>\xi\rangle}{\langle|\widetilde{b}_\perp|^2\,|\mathrm{LIM}>\xi\rangle}, \tag{10}$$

where LIM is the local intermittency measure [67, 76] and ξ is the threshold for the conditional average. We scan a range of different thresholds and study how the results depend on this choice. The LIM is defined as the local wavelet spectrum normalized to its mean at a given scale. Thus, LIM > 1 at the locations where the power spectral density exceeds its mean value. The LIM may be based on different quantities. We use everywhere the same type of LIM so that all conditional averages are constrained to the same spatial locations. In particular, we choose the LIM based on the KAW energy density (see Sec. II): LIM $\equiv \left(|\widetilde{b}_\perp|^2+|\widetilde{n}_e|^2\right)/\left\langle|\widetilde{b}_\perp|^2+|\widetilde{n}_e|^2\right\rangle$. This appears to be a reasonable choice given that the kinetic scale structures carry both significant magnetic field and density fluctuations as shown in what follows. For Cluster measurements, $\delta b_\parallel$ is used as a proxy for δn_e to obtain the LIM under the assumption of pressure balance (6). The conditional averages may eventually become energetically insignificant, since the averaging volume shrinks with the threshold ξ. To focus on the conditional ratios which are still of some energetic relevance, we require for any averaging sub-domain to contain at least 1% of the total KAW energy at that scale. Estimates not satisfying the condition are omitted from the results. The typical volume fractions corresponding to the 1% energy fraction are naturally much smaller than 1%.

The generalized ratios (9)-(10) are compared against the linear predictions (4). In the normalized units (1)-(3), linear KAW theory predicts a numerical value of unity for all ratios considered above in the asymptotic limit (5). From a theoretical point of view, it is not at all evident if the linear predictions are of any relevance for the generalized ratios, which are sensitive to the local, high-amplitude fluctuations and structures related to intermittency. The answer to this intriguing question is the subject of this paper.

IV. RESULTS

We now turn to the main results of this work. First, we characterize the statistical nature of fluctuations separately for each field in terms of the scale-dependent flatness [71]: $F(k_\perp) = \langle|\delta f|^4\rangle/\langle|\delta f|^2\rangle^2$, where $\delta f \in \{\delta n_e, \delta b_\parallel, \delta b_\perp\}$ represents a wavelet decomposed field (sec Sec. III C). For a field with a Gaussian probability distribution, we have $F = 3$. Thus, high values of the flatness above 3 characterize the degree of non-Gaussianity, while a scale-dependence of F points towards intermittency in the classical sense of the term as a departure from self-similarity [77]. The scale-dependent flatness results obtained from solar wind measurements and from the 3D fully kinetic simulation are compared in Fig. 3. To illustrate the statistical uncertainties, we add errorbars to the flatness measurements. To obtain the errorbars, we calculate the moments separately on a number of non-overlapping subsets and then use these as input for a jackknife error estimate of the flatness [78].

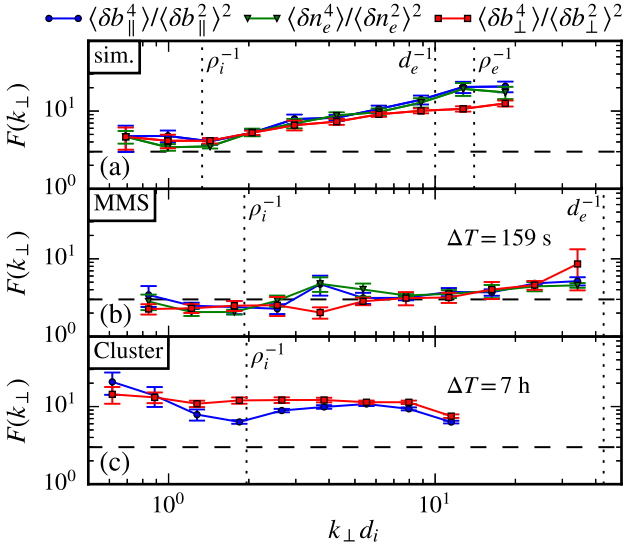

Figure 3. Scale-dependent flatness results obtained from the simulation (a), MMS interval (b), and the Cluster interval (c). Vertical dotted lines mark the plasma kinetic scales and the horizontal dashed lines mark the Gaussian value of 3.

As evident from the results presented in Fig. 3, the kinetic scale fluctuations exhibit clear signatures of non-Gaussian statistics with flatness values above 3. The departure from Gaussian statistics is altogether largest in the Cluster interval, which is to be expected considering that the 7 h interval contains a very large sample of kinetic scale fluctuations. In

agreement with previous works [44, 72], the Cluster statistics are nearly scale-independent at kinetic scales. This is in contrast with the simulation where the flatness is scale-dependent and only gradually increases above the Gaussian value with decreasing scale, presumably due to the finite simulation domain size [79]. All three analyzed fields in the simulation exhibit similar statistical properties, in agreement with the Cluster results for $\delta b_\perp$ and $\delta b_\parallel$ below the ρ_i scale. It is worth pointing out that a previous analysis of density intermittency in the free solar wind [75] found δn_e flatness values comparable to our Cluster results, which do not include the electron density. As already mentioned (see Sec. III B), the MMS interval is too short to allow for a statistically reliable analysis of intermittency and the results are included here for reference. This is confirmed by examining the MMS flatness measurements, which are mostly close to $F \approx 3$ and behave somewhat irregularly as functions of scale. The analyzed interval still includes, however, a few scales where the statistics appear to be non-Gaussian.

Next, we inspect the spatial structure of fluctuations in the simulation. The fluctuations in a given x–y plane are visualized in Fig. 4. In Figs. 4(a)–4(c) we plot the fields in the range $k_\perp d_i = [5, 10]$ by summing up the wavelet decomposed fluctuations in that range [16, 41, 67, 80] using 8 logarithmically spaced scales. Note that $k_\perp d_i = 10$ already corresponds to the electron inertial scale $d_e = 0.1 d_i$ due to the reduced ion-electron mass ratio employed here. The sub-ion scale fluctuations seem to be comprised of a mixture of sheetlike and filamentary patterns. A 3D inspection of the fluctuations (not shown here) confirms that the structures are indeed elongated in the field-parallel direction, consistent with the anisotropy calculation presented in Fig. 2. A quite remarkable feature seen in Fig. 4 is the excellent matching of the δn_e and $\delta b_\parallel$ fluctuation profiles. Although not obvious considering the full range of kinetic effects retained in the simulation, the latter feature can be explained in the context of KAW turbulence as a result of the perpendicular pressure balance (6). In Figs. 4(d)–4(i) we compare the local spectra at $k_\perp d_i = 5$ [Figs. 4(d)–4(f)] and at $k_\perp d_i = 10$ [Figs. 4(g)–4(i)]. The spatial distribution of the spectral energy density is non-uniform and the peaks in the spectra at different scales tend to be concentrated around the same spatial locations. This local coupling across different scales is a characteristic feature of coherent structures [38, 67, 76]. It is also seen that the non-uniformity increases at smaller scales, consistent with the growth of the flatness with $k_\perp$ (Fig. 3). Finally, while the δn_e and $\delta b_\parallel$ spectra match very well, the local $\delta b_\perp$ spectra match the former only in a rather loose sense. This is as well consistent with our theoretical expectations, since no general linear relation exists between $\delta b_\perp$ and δn_e in real space according to the KAW turbulence theory (see Sec. II). The fact that an apparent weak coupling is seen at all points towards the importance of nonlinear effects in shaping the local fluctuations.

To further investigate the perpendicular pressure balance (6), we compute the wavelet cross-coherence [38, 81, 82] between δn_e and $\delta b_\parallel$ in the simulation and for the MMS interval, using the 1D Morlet wavelet transform [68]. High values of cross coherence close to unity indicate a strong local phase synchronization between two signals. To directly compare

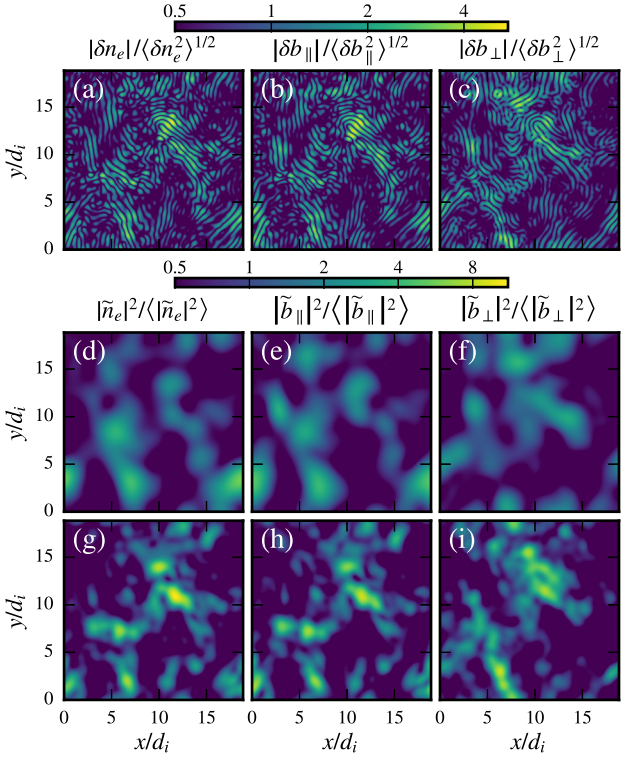

Figure 4. Spatial structure of fluctuations in a given x–y plane in the range $k_\perp d_i = [5, 10]$ (a)–(c), and the (normalized) local wavelet spectra at scale $k_\perp d_i = 5$ (d)–(f) and at scale $k_\perp d_i = 10$ (g)–(i). A logarithmic scale is used to better show also the fluctuations of moderate intensity. Very weak fluctuations with amplitudes below 0.5 in the normalized units are clipped to the lower boundary of the color map.

with spacecraft measurements we construct a 1D trace of simulation data by mimicking a spacecraft fly-through with several passings over the periodic box [83]. In particular, we choose the direction $\hat{\mathbf{n}} = (0.949, 0.292, 0.122)$ and extract the fluctuations along this given direction using cubic spline interpolation. The results are compared in Fig. 5. Arrows are used to show the phase between δn_e and $\delta b_\parallel$. A strong phase synchronization is seen at sub-ion scales of the simulation and of the MMS interval. With most arrows pointing to the left in Fig. 5, the results strongly suggest that δn_e and $\delta b_\parallel$ tend to be anti-correlated and thus fulfill the pressure balance prediction (6) to a good approximation [84]. This conclusion is also in agreement with previous works based on MMS data [46, 82]. We mention that we also checked the coherence between δn_e and (different components of) $\delta b_\perp$. As expected (see Sec. II), δn_e and $\delta b_\perp$ generally do not exhibit a strong cross-coherence (not shown here). However, at rare times of high coherence we often observe a relative phase close to 90 degrees, consistent with the elliptical polarization of the KAW.

Finally, we turn to the central subject of this paper and present the generalized field ratios results. The generalized ratios obtained from the 3D fully kinetic simulation and from spacecraft measurements are plotted in Fig. 6. In Figs. 6(a)–6(f) we show the moment ratios (9) and in Figs. 6(g)–6(l) we

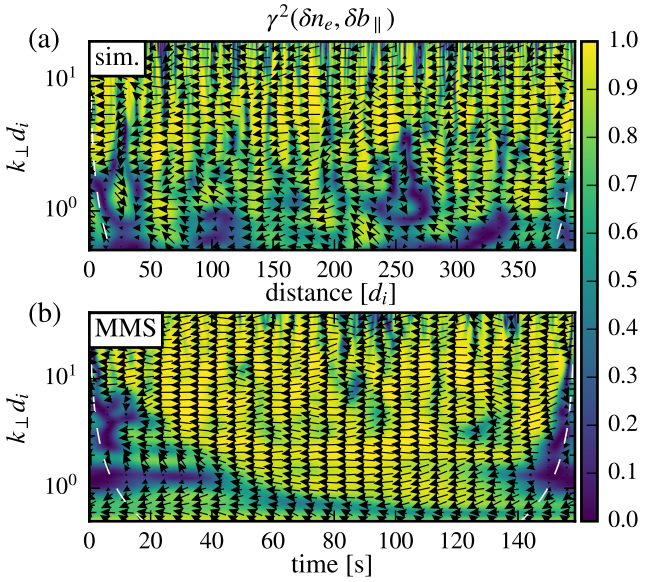

Figure 5. Magnitude squared cross-coherence and phase between δn_e and $\delta b_\parallel$ in the simulation (a) and in the MMS interval (b). The orientation of the arrows (relative to the positive horizontal axis) denotes the phase. Dashed lines show the cone of influence [68].

display the conditional ratios (10), conditioned on the local KAW energy density (see Sec. II and III C). Dashed horizontal lines denote the linear (asymptotic) KAW predictions (4). Dotted vertical lines indicate the characteristic ion and electron scales. The choice $m = 2$ or $\xi = 0$ for the moment ratios and conditional ratios, respectively, yields the standard spectral ratios. We mention that the maximal meaningful threshold ξ (see Sec. III C) grows with $k_\perp$ for the simulation and for MMS data since the fluctuations become more intermittent at smaller scales. The Cluster interval exhibits highly non-Gaussian statistics for all $k_\perp$ (Fig. 3) and thus allows for the use of high thresholds over the whole range. The higher the moment m or threshold ξ, the more sensitive the ratios are to the large-amplitude events. Note that the term "large-amplitude" refers here to the locally enhanced fluctuations and power spectral densities, compared to their scale-dependent mean square values. Spatially, these intense bursts of local activity are not distributed incoherently but instead form distinct patterns (Fig. 4), typically associated with turbulent coherent structures. The locally enhanced, non-Gaussian fluctuations go hand in hand with the non-uniform power spectral densities, since it can be shown that the spatial variability of the energy spectrum and the scale-dependent flatness are directly related [85]. Higher moments assign smaller statistical weights to the lower-amplitude background fluctuations in favor of the large-amplitude events. Similarly, the conditional averages discard the locations with a spectral energy density below the threshold ξ and therefore measure the field ratios within the most energetic structures only.

Altogether, we find a reasonable agreement with linear KAW predictions as well as a good agreement between the simulation and observations. Particularly good agreement with linear theory is found for the generalized ratios of δn_e to $\delta b_\parallel$ [Figs. 6(a)–6(b) and 6(g)–6(h)], which are very close to unity for $k_\perp \gtrsim 1/\rho_i$, regardless of the order m or of the threshold ξ. This is most likely a consequence of the pressure balance (6), which we studied in the preceding paragraphs. It is interesting to note that the ratios tend to converge towards the KAW predictions below the ion gyroradius rather then below the ion inertial scale. This is as well consistent with linear KAW theory, where ρ_i is the relevant transition scale [22, 23]. A reasonable agreement with linear theory is also seen for the δn_e to $\delta b_\perp$ [Figs. 6(c)–6(d) and 6(i)–6(j)] and for the $\delta b_\parallel$ to $\delta b_\perp$ [Figs. 6(e)–6(f) and 6(k)–6(l)] ratios. These two ratios generally agree with linear predictions to order unity and the most energetic structures exhibit a slight tendency to deviate further from linear predictions [see Figs. 6(i)–6(l)], relative to the total ensemble of fluctuations. This implies that kinetic scale structure formation could be a reason for the order unity quantitative deviations from linear predictions often seen in observations and simulations. On the other hand, the deviations attributed to large-amplitude events are altogether only moderate, such that the generalized ratios remain in reasonable agreement with linear predictions. Thus, the wavelike features are not exclusively limited to low-amplitude fluctuations but also carry over to the high-amplitude structures. The agreement between the simulation and the Cluster and MMS intervals suggests that this is an inherent property of the kinetic turbulence rather than a feature specific to the relatively small number of datasets studied here [86]. The observed order unity preservation of linear wavelike properties in kinetic scale turbulent structures constitutes the main result of this work, together with the supplemental evidence presented in Figs. 2–5.

V. DISCUSSION AND CONCLUSIONS

In this paper we employ high-resolution observational data and state-of-the-art computational techniques to study the relationship between wavelike physics and large-amplitude structures in astrophysical kinetic plasma turbulence. Observational results are based on *in situ* solar wind measurements from the Cluster and MMS spacecraft, and the simulation results are obtained from an externally driven, 3D fully kinetic simulation. Our results suggest—in a statistical sense—that the turbulent structures *themselves* approximately preserve linear wave properties. The presence of nonlinear structures is, however, significant and may be a reason for the order unity quantitative deviations from linear predictions often seen in simulations and observations. Furthermore, the simulation results indicate that the intermittency of magnetic field and density fluctuations emerges mainly due to a mixture of pressure-balanced sheets and filaments extending down to electron scales.

The novel analysis presented in this paper implies that the kinetic scale wavelike features and turbulent structure formation are essentially inseparable from each other. As such, our results challenge one of the presently common views of waves and structures "coexistence." The only known framework capable of providing a reasonable theoretical basis for the interpretation of our results appears to be the KAW turbulence phenomenology [21–23]. Known alternatives, such as whistler turbulence

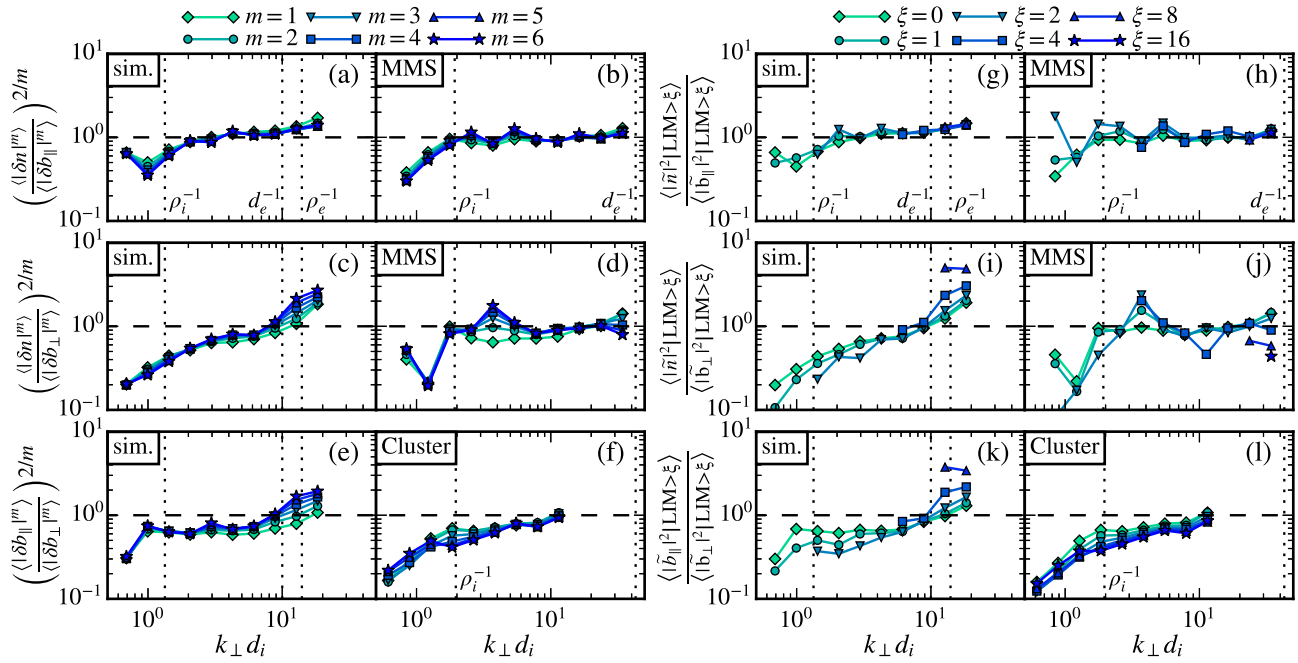

Figure 6. Generalized spectral field ratios obtained from Cluster and MMS measurements and from the 3D fully kinetic simulation (see text for further details). Panels (a)–(f) show the moment ratios (9) and panels (g)–(l) show the conditional ratios (10).

[10, 52–54], cannot explain our results [87]. In this context, an interpretation similar to recent developments in magnetohydrodynamic turbulence [88–91] emerges. Namely, the kinetic scale structures could be perhaps described within the framework of KAW turbulence as the nonlinearly evolving "eddies" of the wavelike turbulent cascade. The possibility that at least a fraction of the sub-ion scale structures are sheetlike, as implied by our simulation results (see also Refs. [28, 32]), lends credence to recent works emphasizing the role of reconnection in sub-ion scale turbulence [37, 92–95], which would require the structures to be sufficiently sheetlike in order to reconnect. In our present understanding, the results of this work do not preclude the reconnection scenario and we intend to explore this aspect in the future.

Finally, we mention that the general approach employed here is not exclusively limited to kinetic range turbulence in astrophysical plasmas and we hope it might find exciting applications in a broad range of turbulent systems where waves and structures have been observed [5–7, 20]. An immediate extension of the method lends itself in the context of inertial range plasma turbulence, where it could be used to study the interplay between structures and waves based on a generalized Alfvén ratio [19, 96].

ACKNOWLEDGMENTS

We gratefully acknowledge helpful conversations with D. Told, A. Bañón Navarro, J. M. TenBarge, and S. S. Cerri. D.G. thanks in particular to N. F. Loureiro for the fruitful exchange of ideas related to this work and for his assistance with obtaining the computing resources, and F. Tsung, V. Decyk, and W. Mori for discussions on particle-in-cell methods and simulations with the OSIRIS code. C.H.K.C. was supported by a Science and Technology Facilities Council (STFC) Ernest Rutherford Fellowship, and A.M. by National Science Foundation (NSF) Grant No. AGS-1624501. K.S. acknowledges support by the French Research Federation for Fusion Studies carried out within the framework of the European Fusion Development Agreement (EFDA). The Cray XC40, Shaheen, at the King Abdullah University of Science & Technology (KAUST) in Thuwal, Saudi Arabia was utilized for all the simulations reported. The authors would like to acknowledge the OSIRIS Consortium, consisting of UCLA and IST (Lisbon, Portugal) for the use of OSIRIS and for providing access to the OSIRIS framework.

[1] E. Quataert and A. Gruzinov, "Turbulence and Particle Heating in Advection-Dominated Accretion Flows," Astrophys. J. **520**, 248 (1999).
[2] S. R. Cranmer and A. A. van Ballegooijen, "Alfvénic Turbulence in the Extended Solar Corona: Kinetic Effects and Proton Heating," Astrophys. J. **594**, 573 (2003).
[3] I. Zhuravleva, E. Churazov, A. A. Schekochihin, S. W. Allen, P. Arévalo, A. C. Fabian, W. R. Forman, J. S. Sanders,

A. Simionescu, R. Sunyaev, A. Vikhlinin, and N. Werner, "Turbulent Heating in Galaxy Clusters Brightest in X-Rays," Nature (London) **515**, 85 (2014).
[4] A. Bañón Navarro, B. Teaca, D. Told, D. Groselj, P. Crandall, and F. Jenko, "Structure of Plasma Heating in Gyrokinetic Alfvénic Turbulence," Phys. Rev. Lett. **117**, 245101 (2016).
[5] E. Yarom and E. Sharon, "Experimental Observation of Steady Inertial Wave Turbulence in Deep Rotating Flows," Nat. Phys. **10**, 510 (2014).
[6] L. Biferale, F. Bonaccorso, I. M. Mazzitelli, M. A. T. van Hinsberg, A. S. Lanotte, S. Musacchio, P. Perlekar, and F. Toschi, "Coherent Structures and Extreme Events in Rotating Multiphase Turbulent Flows," Phys. Rev. X **6**, 041036 (2016).
[7] P. Denissenko, S. Lukaschuk, and S. Nazarenko, "Gravity Wave Turbulence in a Laboratory Flume," Phys. Rev. Lett. **99**, 014501 (2007).
[8] J. A. Krommes, "Fundamental Statistical Descriptions of Plasma Turbulence in Magnetic Fields," Phys. Rep. **360**, 1 (2002).
[9] D. Sundkvist, A. Retinò, A. Vaivads, and S. D. Bale, "Dissipation in Turbulent Plasma due to Reconnection in Thin Current Sheets," Phys. Rev. Lett. **99**, 025004 (2007).
[10] S. P. Gary and C. W. Smith, "Short-Wavelength Turbulence in the Solar Wind: Linear Theory of Whistler and Kinetic Alfvén Fluctuations," J. Geophys. Res. **114**, A12105 (2009).
[11] F. Sahraoui, G. Belmont, and M. L. Goldstein, "New Insight into Short-Wavelenght Solar Wind Fluctuations from Vlasov Theory," Astrophys. J. **748**, 100 (2012).
[12] P. Wu, S. Perri, K. Osman, M. Wan, W. H. Matthaeus, M. A. Shay, M. L. Goldstein, H. Karimabadi, and S. Chapman, "Intermittent Heating in Solar Wind and Kinetic Simulations," Astrophys. J. Lett. **763**, L30 (2013).
[13] C. H. K. Chen, S. Boldyrev, Q. Xia, and J. C. Perez, "Nature of Subproton Scale Turbulence in the Solar Wind," Phys. Rev. Lett. **110**, 225002 (2013).
[14] K. T. Osman, W. H. Matthaeus, J. T. Gosling, A. Greco, S. Servidio, B. Hnat, S. C. Chapman, and T. D. Phan, "Magnetic Reconnection and Intermittent Turbulence in the Solar Wind," Phys. Rev. Lett. **112**, 215002 (2014).
[15] M. Wan, W. H. Matthaeus, V. Roytershteyn, H. Karimabadi, T. Parashar, P. Wu, and M. Shay, "Intermittent Dissipation and Heating in 3D Kinetic Plasma Turbulence," Phys. Rev. Lett. **114**, 175002 (2015).
[16] D. Perrone, O. Alexandrova, A. Mangeney, M. Maksimovic, C. Lacombe, V. Rakoto, J. C. Kasper, and D. Jovanovic, "Compressive Coherent Structures at Ion Scales in the Slow Solar Wind," Astrophys. J. **826**, 196 (2016).
[17] D. Grošelj, A. Mallet, N. F. Loureiro, and F. Jenko, "Fully Kinetic Simulation of 3D Kinetic Alfvén Turbulence," Phys. Rev. Lett. **120**, 105101 (2018).
[18] E. Camporeale, L. Sorriso-Valvo, F. Califano, and A. Retinò, "Coherent Structures and Spectral Energy Transfer in Turbulent Plasma: A Space-Filter Approach," Phys. Rev. Lett. **120**, 125101 (2018).
[19] C. H. K. Chen, "Recent Progress in Astrophysical Plasma Turbulence from Solar Wind Observations," J. Plasma Phys. **82**, 535820602 (2016).
[20] S. Benkadda, T. Dudok de Wit, A. Verga, A. Sen, ASDEX team, and X. Garbet, "Characterization of Coherent Structures in Tokamak Edge Turbulence," Phys. Rev. Lett. **73**, 3403 (1994).
[21] G. G. Howes, S. C. Cowley, W. Dorland, G. W. Hammett, E. Quataert, and A. A. Schekochihin, "A Model of Turbulence in Magnetized Plasmas: Implications for the Dissipation Range in the Solar Wind," J. Geophys. Res. **113**, A05103 (2008).
[22] A. A. Schekochihin, S. C. Cowley, W. Dorland, G. W. Hammett, G. G. Howes, E. Quataert, and T. Tatsuno, "Astrophysical Gyrokinetics: Kinetic and Fluid Turbulent Cascades in Magnetized Weakly Collisional Plasmas," Astrophys. J. Suppl. Ser. **182**, 310 (2009).
[23] S. Boldyrev, K. Horaites, Q. Xia, and J. C. Perez, "Toward a Theory of Astrophysical Plasma Turbulence at Subproton Scales," Astrophys. J. **777**, 41 (2013).
[24] R. A. López, A. F. Viñas, J. A. Araneda, and P. H. Yoon, "Kinetic Scale Structure of Low-Frequency Waves and Fluctuations," Astrophys. J. **845**, 60 (2017).
[25] C. S. Salem, G. G. Howes, D. Sundkvist, S. D. Bale, C. C. Chaston, C. H. K. Chen, and F. S. Mozer, "Identification of Kinetic Alfvén Wave Turbulence in the Solar Wind," Astrophys. J. Lett. **745**, L9 (2012).
[26] J. M. TenBarge, J. J Podesta, K. G. Klein, and G. G. Howes, "Interpreting Magnetic Variance Anisotropy Measurements in the Solar Wind," Astrophys. J. **753**, 107 (2012).
[27] J. M. TenBarge and G. G. Howes, "Current Sheets and Collisionless Damping in Kinetic Plasma Turbulence," Astrophys. J. Lett. **771**, L27 (2013).
[28] S. Kobayashi, F. Sahraoui, T. Passot, D. Laveder, P. L. Sulem, S. Y. Huang, P. Henri, and R. Smets, "Three-Dimensional Simulations and Spacecraft Observations of Sub-Ion Scale Turbulence in the Solar Wind: Influence of Landau Damping," Astrophys. J. **839**, 122 (2017).
[29] S. S. Cerri, S. Servidio, and F. Califano, "Kinetic Cascade in Solar-Wind Turbulence: 3D3V Hybrid-Kinetic Simulations with Electron Inertia," Astrophys. J. Lett. **846**, L18 (2017).
[30] P. Goldreich and S. Sridhar, "Toward a Theory of Interstellar Turbulence. II. Strong Alfvénic Turbulence," Astrophys. J. **438**, 763 (1995).
[31] A. Mallet, A. A. Schekochihin, and B. D. G. Chandran, "Refined Critical Balance in Strong Alfvénic Turbulence," Mon. Not. R. Astron. Soc. **449**, L77 (2015).
[32] S. Boldyrev and J. C. Perez, "Spectrum of Kinetic-Alfvén Turbulence," Astrophys. J. Lett. **758**, L44 (2012).
[33] S. Servidio, F. Valentini, D. Perrone, A. Greco, F. Califano, W. H. Matthaeus, and P. Veltri, "A Kinetic Model of Plasma Turbulence," J. Plasma Phys. **81**, 325810107 (2015).
[34] W. H. Matthaeus, M. Wan, S. Servidio, A. Greco, K. T. Osman, S. Oughton, and P. Dmitruk, "Intermittency, Nonlinear Dynamics and Dissipation in the Solar Wind and Astrophysical Plasmas," Phil. Trans. R. Soc. A **373**, 20140154 (2015).
[35] H. Karimabadi, V. Roytershteyn, M. Wan, W. H. Matthaeus, W. Daughton, P. Wu, M. Shay, B. Loring, J. Borovsky, E. Leonardis, S. C. Chapman, and T. K. M. Nakamura, "Coherent Structures, Intermittent Turbulence, and Dissipation in High-Temperature Plasmas," Phys. Plasmas **20**, 012303 (2013).
[36] A. Chasapis, A. Retinò, F. Sahraoui, A. Vaivads, Yu. V. Khotyaintsev, D. Sundkvist, A. Greco, L. Sorriso-Valvo, and P. Canu, "Thin Current Sheets and Associated Electron Heating in Turbulent Space Plasma," Astrophys. J. Lett. **804**, L1 (2015).
[37] T. D. Phan, J. P. Eastwood, M. A. Shay, J. F. Drake, B. U. Ö. Sonnerup, M. Fujimoto, P. A. Cassak, M. Øieroset, J. L. Burch, R. B. Torbert, A. C. Rager, J. C. Dorelli, D. J. Gershman, C. Pollock, P. S. Pyakurel, C. C. Haggerty, Y. Khotyaintsev, B. Lavraud, Y. Saito, M. Oka, R. E. Ergun, A. Retino, O. Le Contel, M. R. Argall, B. L. Giles, T. E. Moore, F. D. Wilder, R. J. Strangeway, C. T. Russell, P. A. Lindqvist, and W. Magnes, "Electron Magnetic Reconnection Without Ion Coupling in Earth's Turbulent Magnetosheath," Nature (London) **557**, 202 (2018).
[38] S. Lion, O. Alexandrova, and A. Zaslavsky, "Coherent Events and Spectral Shape at Ion Kinetic Scales in the Fast Solar Wind Turbulence," Astrophys. J. **824**, 47 (2016).

[39] C. T. Haynes, D. Burgess, E. Camporeale, and T. Sundberg, "Electron Vortex Magnetic Holes: A Nonlinear Coherent Plasma Structure," Phys. Plasmas **22**, 012309 (2015).

[40] V. Roytershteyn, H. Karimabadi, and A. Roberts, "Generation of Magnetic Holes in Fully Kinetic Simulations of Collisionless Turbulence," Phil. Trans. R. Soc. A **373**, 20140151 (2015).

[41] O. W. Roberts and B. Li, "Kinetic Plasma Turbulence in the Fast Solar Wind Measured by *Cluster*," Astrophys. J. **769**, 58 (2013).

[42] Y. Yang, W. H. Matthaeus, T. N. Parashar, P. Wu, M. Wan, Y. Shi, S. Chen, V. Roytershteyn, and W. Daughton, "Energy Transfer Channels and Turbulence Cascade in Vlasov-Maxwell Turbulence," Phys. Rev. E **95**, 061201(R) (2017).

[43] O. Alexandrova, J. Saur, C. Lacombe, A. Mangeney, J. Mitchell, S. J. Schwartz, and P. Robert, "Universality of Solar-Wind Turbulent Spectrum from MHD to Electron Scales," Phys. Rev. Lett. **103**, 165003 (2009).

[44] K. H. Kiyani, S. C. Chapman, Yu. V. Khotyaintsev, M. W. Dunlop, and F. Sahraoui, "Global Scale-Invariant Dissipation in Collisionless Plasma Turbulence," Phys. Rev. Lett. **103**, 075006 (2009).

[45] F. Sahraoui, M. L. Goldstein, G. Belmont, P. Canu, and L. Rezeau, "Three Dimensional Anisotropic k Spectra of Turbulence at Subproton Scales in the Solar Wind," Phys. Rev. Lett. **105**, 131101 (2010).

[46] D. J. Gershman, A. F.-Viñas, J. C. Dorelli, M. L. Goldstein, J. Shuster, L. A. Avanov, S. A. Boardsen, J. E. Stawarz, S. J. Schwartz, C. Schiff, B. Lavraud, Y. Saito, W. R. Paterson, B. L. Giles, C. J. Pollock, R. J. Strangeway, C. T. Russell, R. B. Torbert, T. E. Moore, and J. L. Burch, "Energy Partitioning Constraints at Kinetic Scales in Low-β Turbulence," Phys. Plasmas **25**, 022303 (2018).

[47] E. Leonardis, S. C. Chapman, W. Daughton, V. Roytershteyn, and H. Karimabadi, "Identification of Intermittent Multifractal Turbulence in Fully Kinetic Simulations of Magnetic Reconnection," Phys. Rev. Lett. **110**, 205002 (2013).

[48] V. Zhdankin, G. R. Werner, D. A. Uzdensky, and M. C. Begelman, "Kinetic Turbulence in Relativistic Plasma: From Thermal Bath to Nonthermal Continuum," Phys. Rev. Lett. **118**, 055103 (2017).

[49] T. J. Dennis and B. D. G. Chandran, "Turbulent Heating of Galaxy-Cluster Plasmas," Astrophys. J. **622**, 205 (2005).

[50] M. W. Kunz, J. M. Stone, and E. Quataert, "Magnetorotational Turbulence and Dynamo in a Collisionless Plasma," Phys. Rev. Lett. **117**, 235101 (2016).

[51] B. M. Gaensler, M. Haverkorn, B. Burkhart, K. J. Newton-McGee, R. D. Ekers, A. Lazarian, N. M. McClure-Griffiths, T. Robishaw, J. M. Dickey, and A. J. Green, "Low-Mach-Number Turbulence in Interstellar Gas Revealed by Radio Polarization Gradient," Nature (London) **478**, 214 (2011).

[52] S. Galtier and A. Bhattacharjee, "Anisotropic Weak Whistler Wave Turbulence in Electron Magnetohydrodynamics," Phys. Plasmas **10**, 3065 (2003).

[53] D. Shaikh and G. P. Zank, "Spectral Features of Solar Wind Turbulent Plasma," Mon. Not. R. Astron. Soc. **400**, 1881 (2009).

[54] S. P. Gary, O. Chang, and J. Wang, "Forward Cascade of Whistler Turbulence: Three-Dimensional Particle-in-Cell Simulations," Astrophys. J. **755**, 142 (2012).

[55] J. Cho and A. Lazarian, "Simulations of Electron Magnetohydrodynamic Turbulence," Astrophys. J. **701**, 236 (2009).

[56] Following Boldyrev *et al.* [23], waves corresponding to the extension of the kinetic Alfvén branch above the ion cyclotron frequency, sometimes referred to as Alfvén-whistler modes [11, 46], would be identified as KAWs rather than whistlers according to (4). These modes, unlike the whistlers emerging as an extension of the fast mode, are essentially pressure balanced and carry significant density fluctuations.

[57] Numerical solutions of the KAW dispersion relation [10, 26, 70] show a slight wave number dependence between the field amplitudes throughout the sub-ion range. We only consider here the asymptotic predictions (4) for simplicity.

[58] P. W. Terry and K. W. Smith, "Coherence and Intermittency of Electron Density in Small-Scale Interstellar Turbulence," Astrophys. J. **665**, 402 (2007).

[59] R. A. Fonseca, L. O. Silva, F. S. Tsung, V. K. Decyk, W. Lu, C. Ren, W. B. Mori, S. Deng, S. Lee, T. Katsouleas, and J. C. Adam, "OSIRIS: A Three-Dimensional, Fully Relativistic Particle in Cell Code for Modeling Plasma Based Accelerators," Lecture Notes in Comput. Sci. **2331**, 342–351 (2002).

[60] R. A. Fonseca, J. Vieira, F. Fiuza, A. Davidson, F. S. Tsung, W. B. Mori, and L. O. Silva, "Exploiting Multi-Scale Parallelism for Large Scale Numerical Modelling of Laser Wakefield Accelerators," Plasma Phys. Control. Fusion **55**, 124011 (2013).

[61] J. M. TenBarge, G. G. Howes, W. Dorland, and G. W. Hammett, "An Oscillating Langevin Antenna for Driving Plasma Turbulence Simulations," Comput. Phys. Commun. **185**, 578–589 (2014).

[62] L. Franci, S. Landi, A. Verdini, L. Matteini, and P. Hellinger, "Solar Wind Turbulent Cascade from MHD to Sub-Ion Scales: Large-Size 3D Hybrid Particle-in-Cell Simulations," Astrophys. J. **853**, 26 (2018).

[63] C. P Escoubet, M. Fehringer, and M. Goldstein, "*Introduction* The Cluster Mission," Ann. Geophys. **19**, 1197 (2001).

[64] J. L. Burch, T. E. Moore, R. B. Torbert, and B. L. Giles, "Magnetospheric Multiscale Overview and Science Objectives," Space Sci. Rev. **199**, 5 (2016).

[65] C. H. K. Chen, L. Matteini, D. Burgess, and T. S. Horbury, "Magnetic Field Rotations in the Solar Wind at Kinetic Scales," Mon. Not. R. Astron. Soc. **453**, L64 (2015).

[66] G. G. Howes, K. G. Klein, and J. M. TenBarge, "Validity of the Taylor Hypothesis for Linear Kinetic Waves in the Weakly Collisional Solar Wind," Astrophys. J. **789**, 106 (2014).

[67] M. Farge, "Wavelet Transforms and their Applications to Turbulence," Annu. Rev. Fluid Mech. **24**, 395 (1992).

[68] C. Torrence and G. P. Compo, "A Practical Guide to Wavelet Analysis," Bull. Am. Meteorol. Soc. **79**, 61 (1998).

[69] J. F. Kirby, "Which Wavelet Best Reproduces the Fourier Power Spectrum?" Comput. Geosci. **31**, 846 (2005).

[70] D. Grošelj, S. S. Cerri, A. Bañón Navarro, C. Willmott, D. Told, N. F. Loureiro, F. Califano, and F. Jenko, "Fully Kinetic versus Reduced-Kinetic Modeling of Collisionless Plasma Turbulence," Astrophys. J. **847**, 28 (2017).

[71] M. Farge and K. Schneider, "Wavelet Transforms and their Applications to MHD and Plasma Turbulence: A Review," J. Plasma Phys. **81**, 435810602 (2015).

[72] K. H. Kiyani, S. C. Chapman, F. Sahraoui, B. Hnat, O. Fauvarque, and Yu. V. Khotyaintsev, "Enhanced Magnetic Compressibility and Isotropic Scale Invariance at Sub-Ion Larmor Scales in Solar Wind Turbulence," Astrophys. J. **763**, 10 (2013).

[73] T. Dudok de Wit, "Can High-Order Moments be Meaningfully Estimated from Experimental Turbulence Measurements?" Phys. Rev. E **70**, 055302(R) (2004).

[74] K. Kiyani, S. C. Chapman, and B. Hnat, "Extracting the Scaling Exponents of a Self-Affine, Non-Gaussian Process from a Finite-Length Time Series," Phys. Rev. E **74**, 051122 (2006).

[75] C. H. K. Chen, L. Sorriso-Valvo, J. Šafránková, and Z. Němeček, "Intermittency of Solar Wind Density Fluctuations from Ion to Electron Scales," Astrophys. J. Lett. **789**, L8 (2014).

[76] J. Ruppert-Felsot, M. Farge, and P. Petitjeans, "Wavelet Tools

to Study Intermittency: Application to Vortex Bursting," J. Fluid Mech. **636**, 427 (2009).
[77] U. Frisch, *Turbulence: The Legacy of A. N. Kolmogorov* (Cambridge University Press, Cambridge, 1995).
[78] J. Shao and D. Tu, *The Jackknife and Bootstrap* (Springer, New York, 1995).
[79] Note that the flatness may depend to some degree on the details of the scale decomposition. Applying the 1D Morlet transform to the simulation data, we obtain a somewhat lower but qualitatively similar flatness, reaching about $F \approx 6$ at the smallest scales.
[80] J. He, C. Tu, E. Marsch, and S. Yao, "Do Oblique Alfvén/Ion-Cyclotron or Fast-Mode/Whistler Waves Dominate the Dissipation of Solar Wind Turbulence Near the Proton Inertial Length?" Astrophys. J. Lett. **745**, L8 (2012).
[81] A. Grinsted, J. C. Moore, and S. Jevrejeva, "Application of the Cross Wavelet Transform and Wavelet Coherence to Geophysical Time Series," Nonlinear Proc. Geoph. **11**, 561 (2004).
[82] C. H. K. Chen and S. Boldyrev, "Nature of Kinetic Scale Turbulence in the Earth's Magnetosheath," Astrophys. J. **842**, 122 (2017).
[83] A. Greco, P. Chuychai, W. H. Matthaeus, S. Servidio, and P. Dmitruk, "Intermittent MHD Structures and Classical Discontinuities," Geophys. Res. Lett. **35**, L19111 (2008).
[84] A few events, mostly around the d_i scale, are seen in the simulation where either the cross-coherence is low or where the phase between δn_e and $\delta b_\parallel$ significantly differs from 180 degrees. There could be several reasons for this. An interesting possibility pertains to the role of kinetic instabilities [97] or fast magnetosonic waves, which violate pressure balance. On the other hand, a simpler explanation could be that the fluctuations (especially at large scales) are generally too large to allow for a linearization of the magnetic pressure [22] around its local background value.
[85] W. J. T. Bos, L. Liechtenstein, and K. Schneider, "Small-Scale Intermittency in Anisotropic Turbulence," Phys. Rev. E **76**, 046310 (2007).
[86] To test the robustness of the agreement, we computed the generalized ratios by applying the 1D instead of the 2D Morlet transform to the simulation data. The 1D transform gives qualitatively very similar results and leads essentially to the same conclusions.
[87] See Refs. [13, 23, 82] for discussions on the differences between KAW and whistler wave turbulence. Essentially, whistlers carry only minor density fluctuations and do not fulfill the pressure balance (6). In a $\beta \sim 1$ plasma they are also expected to be rather strongly damped for $k_\parallel d_i \lesssim 1$, which contradicts our results in Fig. 2.
[88] S. Boldyrev, "Spectrum of Magnetohydrodynamic Turbulence," Phys. Rev. Lett. **96**, 115002 (2006).
[89] A. Mallet, A. A. Schekochihin, B. D. G. Chandran, C. H. K. Chen, T. S. Horbury, R. T. Wicks, and C. C. Greenan, "Measures of Three-Dimensional Anisotropy and Intermittency in Strong Alfvénic Turbulence," Mon. Not. R. Astron. Soc. **459**, 2130 (2016).
[90] G. G. Howes, "The Dynamical Generation of Current Sheets in Astrophysical Plasma Turbulence," Astrophys. J. Lett. **827**, L28 (2016).
[91] A. Mallet and A. A. Schekochihin, "A Statistical Model of Three-Dimensional Anisotropy and Intermittency in Strong Alfvénic Turbulence," Mon. Not. R. Astron. Soc. **466**, 3918 (2017).
[92] S. S. Cerri and F. Califano, "Reconnection and Small-Scale Fields in 2D-3V Hybrid-Kinetic Driven Turbulence Simulations," New J. Phys. **19**, 025007 (2017).
[93] A. Mallet, A. A. Schekochihin, and B. D. G. Chandran, "Disruption of Alfvénic Turbulence by Magnetic Reconnection in a Collisionless Plasma," J. Plasma Phys. **83**, 905830609 (2017).
[94] N. F. Loureiro and S. Boldyrev, "Collisionless Reconnection in Magnetohydrodynamic and Kinetic Turbulence," Astrophys. J. **850**, 182 (2017).
[95] L. Franci, S. S. Cerri, F. Califano, S. Landi, E. Papini, A. Verdini, L. Matteini, F. Jenko, and P. Hellinger, "Magnetic Reconnection as a Driver for a Sub-Ion-Scale Cascade in Plasma Turbulence," Astrophys. J. Lett. **850**, L16 (2017).
[96] C. Salem, A. Mangeney, S. D. Bale, and P. Veltri, "Solar Wind Magnetohydrodynamics Turbulence: Anomalous Scaling and Role of Intermittency," Astrophys. J. **702**, 537 (2009).
[97] M. W. Kunz, I. G. Abel, K. G. Klein, and A. A. Schekochihin, "Astrophysical Gyrokinetics: Turbulence in Pressure-Anisotropic Plasmas at Ion Scales and Beyond," J. Plasma Phys. **84**, 715840201 (2018).